

# How the absorber thickness influences the formation of reverse bias induced defects in CIGS solar cells

Klaas Bakker<sup>1,2,\*</sup>, Alix Rasia<sup>1</sup>, Suzanne Assen<sup>1</sup>, Basma Ben Said Aflouat<sup>1</sup>, Arthur Weeber<sup>2,3</sup>, and Mirjam Theelen<sup>1</sup>

<sup>1</sup> TNO - Solliance, High Tech Campus 21, 5656 AE, Eindhoven, The Netherlands

<sup>2</sup> Delft University of Technology, PhotoVoltaic Materials and Devices (PVMD), Mekelweg 4, 2628 CD, Delft, The Netherlands

<sup>3</sup> TNO Energy Transition – Solar Energy, Westerduinweg 3, 1755 LE, Petten, The Netherlands

Received: 15 July 2020 / Received in final form: 28 September 2020 / Accepted: 8 October 2020

**Abstract.** When a PV module is partially shaded, the shaded solar cells operate in a reverse bias condition. For Cu(In,Ga)Se<sub>2</sub> cells this condition can cause defects that irreversibly reduce the output of these cells and the full module. In order to design robust shade-tolerant CIGS modules details need to be known of the conditions at which these defects will be formed. In this study a large number of cells were exposed to different reverse bias conditions. By using simple statistics the probability of the occurrence of defects as a result of reverse bias at any given voltage has been determined. Based on our experiments we have found that the absorber thickness is one of the main parameters that affects the shade-tolerance: the thicker the absorber, the more shade tolerant the CIGS module will be.

**Keywords:** CIGS / partial shading / reverse bias / wormlike defects / reliability

## 1 Introduction

Partial shading of photovoltaic (PV) modules can lead to reverse bias voltages in the shaded cells. In Cu(In,Ga)Se<sub>2</sub> (CIGS) modules this reverse bias condition can lead to the formation of reverse bias induced defects or wormlike defects [1]. Wormlike defects act as local shunts and permanently reduce the output of a PV module. Mitigation against reverse bias damage is often obtained by the integration of bypass diodes, especially in wafer-based crystalline silicon PV modules this is standard practice. However, the integration of bypass diodes in monolithically interconnected CIGS modules, the most commonly used type of CIGS modules, is almost impossible. Another possible mitigation option against reverse bias damage in CIGS is to utilize the CIGS solar cell itself as a bypass diode, as proposed by Silverman et al. [2]. This would be feasible because the reverse characteristic of a CIGS solar cell shows a very steep incline in reverse current, like a Zener or Avalanche breakdown [3,4]. From literature it is known that both the buffer layer thickness and composition have a strong impact on the reverse characteristic [4–6], as well as the sodium content in the absorber layer [3,7]. On the other hand, it has been observed that the absorber layer

thickness does not have a large influence on the reverse characteristic [8]. In order to successfully utilize the CIGS cell as a bypass diode, the formation of wormlike defects should be prevented and therefore the reverse characteristic needs to be shifted to stay below the damage threshold. Recent studies presented in references [8,9] on the threshold conditions at which wormlike defects are formed are not conclusive and show huge variations in results. In this study a large number of cells with varying absorber layer thicknesses have been exposed to extreme conditions in order to determine the impact of reverse bias on cell performance and simultaneously obtain sufficient statistics.

## 2 Experimental

The CIGS solar cells were fabricated using the three stage co-evaporation process [10]. The layer stack consists of: 400 nm direct current (DC) sputtered Mo, CIGS with varying thickness and composition, 50 nm chemical bath deposited CdS, 60 nm DC sputtered intrinsic zinc oxide, 210 nm DC sputtered aluminum-doped zinc-oxide and a metal current-collecting grid (20 nm Ni, 600 nm Ag, 20 nm Ni) applied with e-beam evaporation. These layer stacks were deposited on 1 mm soda lime glass (SLG) substrates with a dimension of 100 × 100 mm<sup>2</sup> and manually divided in 162 individual cells, each with a dimension of approximately 5 × 10 mm<sup>2</sup>, with a scalpel.

\* e-mail: [klaas.bakker@solliance.eu](mailto:klaas.bakker@solliance.eu)

**Table 1.** List of substrates used including for each substrate the average absorber thickness, solar cell efficiency, and damage voltage for both the dark (DRB) and illuminated (LRB) reverse bias sweeps. The average values are based on at least 22 measurement points per substrate, the error bar presented is the standard deviation. Several values are missing in the last column (damage voltage in LRB), due to the low number of damaged cells ( $n < 20$ ) needed to give a reliable estimate. The table also displays the damage ratio in both dark reverse bias and illuminated reverse bias, together with the number of cells ( $n$ ) used to calculate this ratio.

Substrate	Absorber thickness [nm]	Efficiency [%]	$n$ cells DRB	DRB damage ratio [%]	DRB damage voltage [V]	$n$ cells LRB	LRB damage ratio [%]	LRB damage voltage [V]
Group I-a	$262 \pm 12$	$7.3 \pm 0.4$	76	100%	$-2.5 \pm 0.4$	22	100%	$-2.4 \pm 0.7$
Group I-b	$433 \pm 22$	$9.9 \pm 0.5$	27	100%	$-2.7 \pm 1.0$	35	100%	$-3.0 \pm 0.2$
Group I-c	$468 \pm 23$	$8.0 \pm 0.4$	60	100%	$-2.9 \pm 0.4$	43	98%	$-2.7 \pm 0.3$
Group I-d	$503 \pm 25$	$9.7 \pm 0.4$	73	100%	$-3.0 \pm 0.6$	43	100%	$-3.2 \pm 0.4$
Group I-e	$517 \pm 25$	$9.0 \pm 0.3$	76	100%	$-2.9 \pm 0.7$	50	100%	$-3.2 \pm 0.5$
Group I-f	$889 \pm 45$	$13.6 \pm 0.4$	78	92%	$-3.7 \pm 1.1$	24	42%	
Group II-a	$545 \pm 10$	$11.7 \pm 0.4$	47	100%	$-4.0 \pm 0.9$	17	12%	
Group II-b	$580 \pm 10$	$11.6 \pm 0.7$	51	96%	$-3.9 \pm 0.8$	28	21%	
Group II-c	$586 \pm 11$	$11.4 \pm 0.4$	69	94%	$-3.9 \pm 0.8$	34	38%	
Group III-a	$1567 \pm 37$	$13.2 \pm 1.1$	36	97%	$-4.7 \pm 0.7$	35	11%	
Group III-b	$1585 \pm 39$	$13.6 \pm 1.5$	36	97%	$-4.6 \pm 0.6$	36	6%	
Group III-c	$1696 \pm 47$	$12.2 \pm 0.9$	36	100%	$-6.7 \pm 2.4$	35	6%	
Group III-d	$1721 \pm 38$	$13.2 \pm 0.9$	35	100%	$-7.8 \pm 1.9$	36	0%	
Group III-e	$1787 \pm 38$	$13.7 \pm 0.5$	35	91%	$-7.6 \pm 1.8$	32	3%	
Group III-f	$1910 \pm 43$	$15.3 \pm 1.2$	36	97%	$-6.7 \pm 2.0$	31	0%	

In this study three groups of cells were used:

- Group I: 6 substrates, absorber thickness varying between 237 and 965 nm. The composition and thickness distribution for this group is less uniform than the other two groups. Furthermore, the reverse bias measurements were performed 5 months after fabrication with a slightly lower scan speed than the other two groups.
- Group II: 3 substrates, thickness between 524 and 604 nm. Furthermore 5 nm of NaF was evaporated before CIGS deposition, to increase the initial efficiency.
- Group III: 6 substrates, thickness between 1479 and 1984 nm.

The average thicknesses of the individual substrates are included in [Table 1](#).

$JV$  measurements were performed in an automated setup that measures both in darkness and under illumination. As illumination source a Newport Xenon lamp with AM1.5 filter was used. To perform the  $JV$  sweeps in forward and reverse a Keithley 2400 source measure unit (SMU) was used. The SMU was set to automatically change the current range and the current compliance was set to 100 mA ( $200 \text{ mA/cm}^2$ ). The voltage step used for all  $JV$  sweeps was 20 mV, with the exception of the reverse sweep of group I which was 10 mV. For the reverse  $JV$  sweeps in the dark (DRB) the start voltage was +0.72 V and end voltage was  $-6$  or  $-15$  V for the substrates of group I and II and group III, respectively. For the illuminated reverse  $JV$  sweeps (LRB) the start and end voltages were +0.72 and  $-6$  V, respectively.

The calculations of average, standard deviation and normal distribution were performed with the built-in functions of Excel. The damage parameters are determined from the derivative curve using a Matlab script that had a manual control and correction option build in.

### 3 Results

In general, the formation of a wormlike defect during the  $JV$  sweep is accompanied by a sudden sharp increase in current [11] of which an example is given in [Figure 1](#). At the moment the sudden sharp increase in current occurs, the cell will be irreversibly damaged. The parameters at this point are labeled as damage voltage and damage current density. Since not all cells got damaged by the sweep a damage ratio was defined as the number of damaged cells divided by the number of cells measured. A cell is considered to be damaged in the analysis in case the fill factor has been reduced by more than 3% relative. Cells that were bad ( $< 0.85$  times the efficiency of 11th best cell) before the reverse bias sweep were excluded from the statistical analysis. The average results of the damaged cells of each substrate are summarized in [Table 1](#). Two clear trends can directly be observed from this table. First, the damage voltage in DRB shifts to lower negative voltages with increasing layer thickness. Second, the damage ratio in darkness and under illumination are different. The LRB damage ratio is decreasing with increasing absorber layer thickness. Furthermore, for the

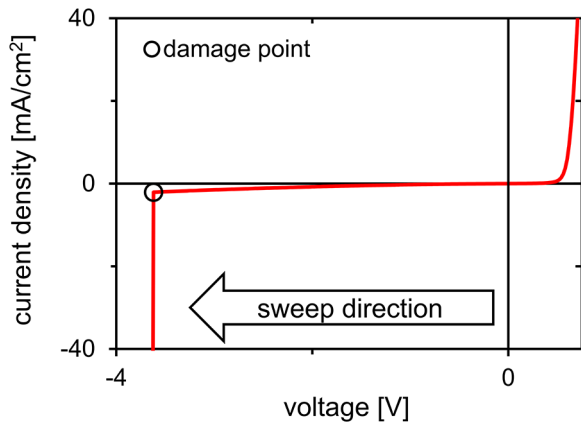


**Fig. 1.** *JV* graph of a cell that was damaged during the *JV* sweep. The moment when the cell was damaged and a wormlike defect started to form is accompanied by a sharp increase in current. This damage point is indicated with a black circle in the graph.

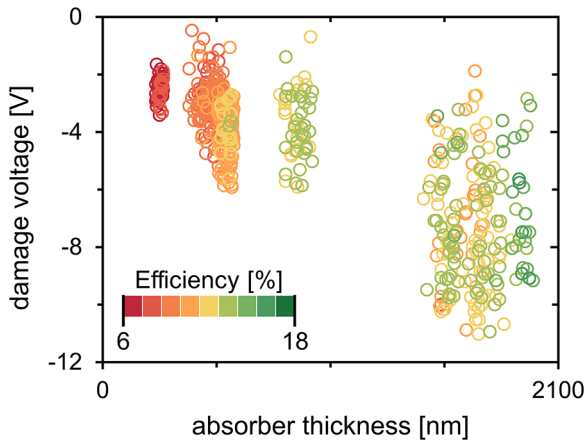


**Fig. 2.** Damage voltage for dark reverse bias as function of absorber thickness. The initial efficiency of the individual solar cells is represented with a color scale.

substrates with thicker absorbers almost no cells got damaged under illumination. In order to examine the trend in the DRB damage voltage for the individual cells, the damage voltage in DRB is plotted against the absorber thickness and presented in Figure 2. The efficiency is added in a color scale, and can be seen as an additional dimension to the plot. From this plot it is evident that there is a large variation in damage voltage, which was also observed by Mansfield et al. [8] and Richter et al. [9].

The variations for the three groups of substrates including their fitting to normal distribution curves are plotted in the histograms of Figure 3. In order to validate if this normal distribution additional DRB measurements until  $-6$  V were performed on 425 cells of the group III substrates. The measured damage ratio of the *JV* sweep until  $-6$  V is 28.0%, while the damage probability calculated from the normal distribution in Figure 3, is

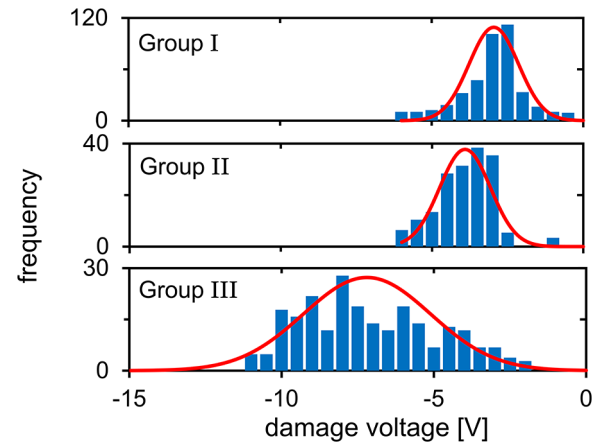


**Fig. 3.** Histograms of damage voltage in dark reverse bias sweep and the normal distribution curve based on average and standard deviation for all three groups of substrates.

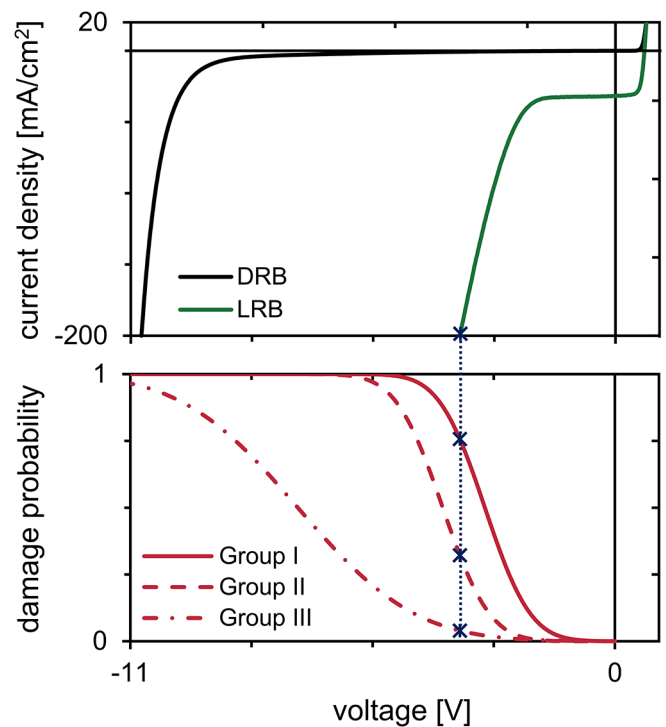


**Fig. 4.** The top graph shows typical *JV* curves of illuminated and dark reverse characteristic. The red curves plotted on the bottom graph represent the damage probability in the dark. The damage probability is the accumulated normal distribution from DRB measurements, a damage probability of 1 means a 100% chance of failure due to reverse bias. The blue dotted line shows the voltage at the current limit of the LRB *JV* curve.

28.4%. Because these two percentages are in very good agreement we propose that fitting the occurrence of failure to a normal distribution can be used to determine the probability of having cells damaged due to reverse bias at any given voltage.

Figure 4 shows a typical reverse *JV* curve in the dark and under illumination together with the damage probability curve in the dark for each group of cells. From this

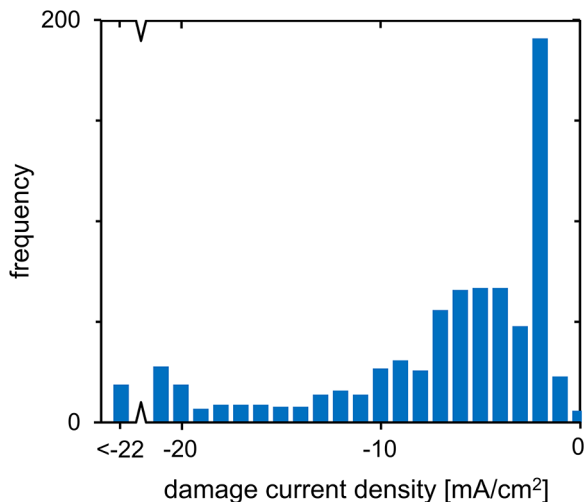


**Fig. 5.** Histogram of damage current density in dark reverse bias sweeps for all samples. The last bin (most left) represents the total number of cells with a damage current density smaller than  $-22 \text{ mA/cm}^2$ .

figure it can be seen that the reverse curves under illumination and in darkness are completely different. Both curves have a steep incline in current, however, this transition happens at much higher negative voltages in the dark. This behavior is also observed by references [3,5]. One possible strategy to reduce reverse bias damage is to shift this transition to more positive voltages. All cells used in this study have a very late transition in the dark ( $< -6 \text{ V}$ ). However, the illuminated curves can be used in order to assess if a shift of the transition towards a more positive voltage reduces the probability of reverse bias damage.

The SMU is limiting the current density to  $200 \text{ mA/cm}^2$ , therefore the voltage during the sweep cannot exceed the voltage at  $200 \text{ mA/cm}^2$ . As an example, the voltage at  $200 \text{ mA/cm}^2$  is  $-3.5 \text{ V}$  when using the illuminated curve from Figure 4. The calculated damage probabilities at  $-3.5 \text{ V}$  are 74.9%, 31.3% and 3.9% for group I, group II and group III, respectively. These numbers agree well with the actual damage ratios for group II and III, especially when considering that there is also a large variation in the voltages at  $200 \text{ mA/cm}^2$ . The results of group I are influenced by the substrate Group I-f, this substrate has a thicker absorber and thus a much lower average damage voltage and damage ratio.

A closer inspection of the current densities at which the cells fail is given in the histogram of Figure 5. This histogram shows that a large number of cells got damaged at current densities of  $-2$  and  $-20 \text{ mA/cm}^2$ . This coincides with the change in measurement range of the SMU (1 and  $10 \text{ mA}$ ). This implies that the SMU could have an influence on the damage voltage. Because of the loss of measurement accuracy at a fixed current range, the SMU was not set to a fixed current range. Additional measurements (Appendix A) showed that the average damage voltage shifts less than  $0.5 \text{ V}$  when a fixed current range is used instead of a changing. Furthermore, there is a good agreement between dark and illuminated damage voltage

while there is no changeover during illuminated measurements due to the additional light generated current. These observations give sufficient confidence in the validity of the damage voltage determined from reverse  $JV$  sweeps with a SMU that is set to automatically change the current range.

The value of  $200 \text{ mA/cm}^2$  to limit the current density is much higher than realistically can be expected in real life modules. However, this value does indicate the robustness of the cells, especially given the low damage ratios in the group III illuminated reverse bias measurements. Figure 5 reveals that only 15 out of the 676 cells exhibit a damage current exceeding  $22 \text{ mA/cm}^2$  absolute. This indicates that the damage mostly appears in the flat part of the curve. Combined with both the relation of the damage voltage in the dark and the damage ratio under illumination with absorber thickness makes us conclude that the mechanism for damage is voltage driven rather than current.

## 4 Discussion

In the result section it is described that the formation of wormlike defects is a voltage driven process and that there is a correlation between the damage voltage in the dark and the absorber thickness. The reason for thinner cells to be more prone to damage might be inherent to the layer thickness but can also be an indirect consequence of the absorber growth process. For example, sodium concentration, gallium gradient and grain size distribution could all be different for thinner absorbers.

An inherent difference between absorbers with different layer thickness is the internal electric field. This is the applied potential difference between the front and back electrode distributed over the absorber layer. The exact distribution is hard to predict and requires extensive electrical device modeling. Mansfield et al. [8] hypothesized that the enhanced electric field in devices with thin absorbers would assist the tunneling mechanism responsible for the transition in the reverse curve. Therefore, thinning the absorber would alter the reverse characteristic to have an earlier transition, limiting the voltage and preventing damage by reverse bias. Their study showed no correlation between transition and layer thickness. However, they have found an apparent correlation between damage voltage in the dark and absorber layer thickness. In this respect, the results of Mansfield et al. are in agreement with the results presented in this study, even though Mansfield et al. described “the trend to be not perfect”. In this study, a large number of devices have been measured, in order to obtain more confidence in the results. It is likely that the enhanced electric field in thinner absorbers is at least partly responsible for the increased sensitivity to reverse bias damage.

Besides the electric field, other factors, mostly related to device characteristics, change as well when making the absorber thinner. A major factor is the reduced absorption in thinner absorbers, which is responsible for the reduced  $J_{sc}$  observed for thinner cells. However, this is not expected to directly influence the damage voltage in darkness. Changes in device quality, due for example to enhanced

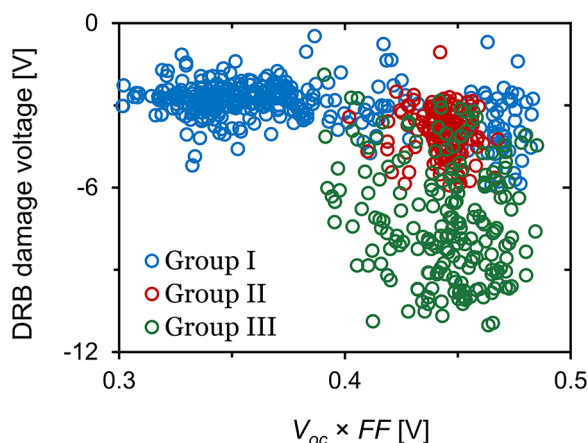


**Fig. 6.** Plot of all cells of groups I, II and III, that were damaged during a dark reverse bias sweep. On the  $x$ -axis the  $V_{oc} \times FF$  value, and on the  $y$ -axis the damage voltage in the dark is plotted.

recombination at the back contact, often result in reduced  $V_{oc}$  and  $FF$ . The product of the  $V_{oc}$  and  $FF$  is therefore a good metric to assess the quality of the device. Figure 6 shows the  $V_{oc} \times FF$  value for all the cells that were damaged during dark reverse bias sweeps. This figure shows a very large spread as well as a large number of cells with a low  $V_{oc} \times FF$  value in group I. The lower efficiency of the group I cells was the initial motivation to add group II, with higher efficiency cells and thin absorbers, to this study. As can be observed in Figure 6 the  $V_{oc} \times FF$  value for group II are in the same range as group III (cells with thicker absorbers). From the difference between group I and II in terms of  $V_{oc} \times FF$  values and damage voltage in the dark, it can be concluded that the device quality could be a factor contributing to the damage voltage. However, group II and III show different damage voltage but similar  $V_{oc} \times FF$ , which suggests that the absorber layer thickness is probably the dominant factor for the damage voltage in the dark.

Another factor is the structural quality of the device itself. It is known that wormlike defects often originate at local weak spots, such as small pits, craters and cracks [12,13]. It could be expected that during the growth of the absorber layer the material quality improves. Therefore, more of these defects could be expected in thinner cells. However, 84% (683 from the 812) of the wormlike defects found in the group I cells originated at the mechanically defined border. This indicates that, although wormlike defects do originate from local weak spots, these weak spots are likely mechanically induced rather than the result of imperfect absorber growth.

## 5 Conclusions

A large number of CIGS solar cells were exposed to reverse bias conditions in darkness or under illumination. It was demonstrated that the absorber layer thickness has a large

influence on the voltage at which reverse bias induced defects are formed in CIGS cells and irreversibly damage the cells. Under illumination the damage ratio is influenced by the absorber thickness, where cells with thinner absorber layers are more prone to damage. In the dark the absorber thickness has a relation to the voltage at which wormlike defects are formed, thicker cells get damaged at higher absolute voltages. From the measurements in the dark the probability of the formation of wormlike defects at any reverse bias voltage could be estimated using simple statistics. It was shown that the damage probability for illuminated reverse bias estimated using the normal distribution of the measurements in the dark was in good agreement with the actual measured values.

This work is supported by ‘Netherlands Enterprise Agency’ (RVO) and the Dutch Topteam Energy via the project ‘Performance and Electroluminescence Analysis on Reliability and Lifetime of Thin-Film Photovoltaics’ with grant number TEUE116203. Furthermore, the Early Research Program ‘Sustainability & Reliability for solar and other (opto-)electronic thin-film devices’ from TNO is acknowledged for funding.

## Author contribution statement

K. B. prepared the solar cells. K. B., A. R., S. A. and B. B. S. A. performed and analyzed the measurements. K. B. wrote the manuscript in consultation with M. T. and A. W.

## References

1. K. Bakker, A. Weeber, M. Theelen, J. Mater. Res. **34**, 3977 (2019)
2. T.J. Silverman, L. Mansfield, I. Repins, S. Kurtz, IEEE J. Photovolt. **6**, 1333 (2016)
3. S. Puttnins, S. Jander, A. Wehrmann, G. Benndorf, M. Stölzel, A. Müller, H. von Wenckstern, F. Daume, A. Rahm, M. Grundmann, Sol. Energy Mater. Sol. Cells **120**, 506 (2014)
4. P. Szaniawski, P. Zabierowski, J. Olsson, U. Zimmermann, M. Edoff, IEEE J. Photovoltaics **7**, 1136 (2017)
5. P. Szaniawski, J. Lindahl, T. Törndahl, U. Zimmermann, M. Edoff, Thin Solid Films **535**, 326 (2013)
6. S. Puttnins, S. Jander, K. Pelz, S. Heinker, F. Daume, A. Rahm, A. Braun, M. Grundmann, in *26th European Photovoltaic Solar Energy Conference and Exhibition, 2011*, pp. 2432–2434
7. S. Puttnins, M. Purfurst, M. Hartung, H.K. Lee, F. Daume, L. Hartmann, A. Rahm, A. Braun, M. Grundmann, in *27th European Photovoltaic Solar Energy Conference and Exhibition, 2012*, pp. 2219–2221
8. L.M. Mansfield, K. Bowers, S. Glynn, I.L. Repins, in *2019 IEEE 46th Photovoltaic Specialists Conference, 2019*
9. J.P.M. Richter, M. Vrenegor, in *33rd European Photovoltaic Solar Energy Conference and Exhibition, 2017*, pp. 1017–1019

10. A.M. Gabor, J.R. Tuttle, D.S. Albin, M.A. Contreras, R. Noufi, A.M. Hermann, *Appl. Phys. Lett.* **65**, 198 (1994)
11. K. Bakker, H.N. Åhman, T. Burgers, N. Barreau, A. Weeber, M. Theelen, *Sol. Energy Mater. Sol. Cells* **205**, 110249 (2020)
12. E. Palmiotti, S. Johnston, A. Gerber, H. Guthrey, A. Rockett, L. Mansfield, T.J. Silverman, M. Al-Jassim, *Sol. Energy* **161**, 1 (2018)
13. H. Guthrey, M. Nardone, S. Johnston, J. Liu, A. Norman, J. Moseley, M. Al-Jassim, *Prog. Photovolt. Res. Appl.* **27**, 812 (2019)

**Cite this article as:** Klaas Bakker, Alix Rasia, Suzanne Assen, Basma Ben Said Aflouat, Arthur Weeber, Mirjam Theelen, How the absorber thickness influences the formation of reverse bias induced defects in CIGS solar cells, *EPJ Photovoltaics* **11**, 9 (2020)

## Appendix A: Additional measurements comparing fixed and auto-change current range setting

Comparison of results of measurements with SMU set to fixed current range of 100 mA and on auto-change. The main parameters of the substrate used for this

comparison can be found in [Table A.1](#). The histograms for both types of measurements for both damage current density and damage voltage can be found in [Figure A.1](#)

**Table A.1.** Parameters of additional substrate, including the average absorber thickness, solar cell efficiency and damage voltage for both the dark (DRB) reverse bias sweeps with auto-change and fixed current range. The average values are based on more than 30 measurement points per substrate, the error is the standard deviation. Also in the table is the percentage of cells that were damaged in sweeps with auto-change and fixed current range together with the number of cells ( $n$ ) used to calculate this damage ratio.

Substrate	Absorber thickness [nm]	Efficiency [%]	$n$ cells DRB auto-change	DRB auto-change damage ratio [%]	DRB auto-change $V_{\text{damage}}$ [V]	$n$ cells DRB fixed-range	DRB fixed-range damage ratio [%]	DRB fixed-range $V_{\text{damage}}$ [V]
Additional	$1774 \pm 32$	$13.6 \pm 0.6$	48	83%	$-5.8 \pm 1.6$	47	68%	$-6.2 \pm 1.4$

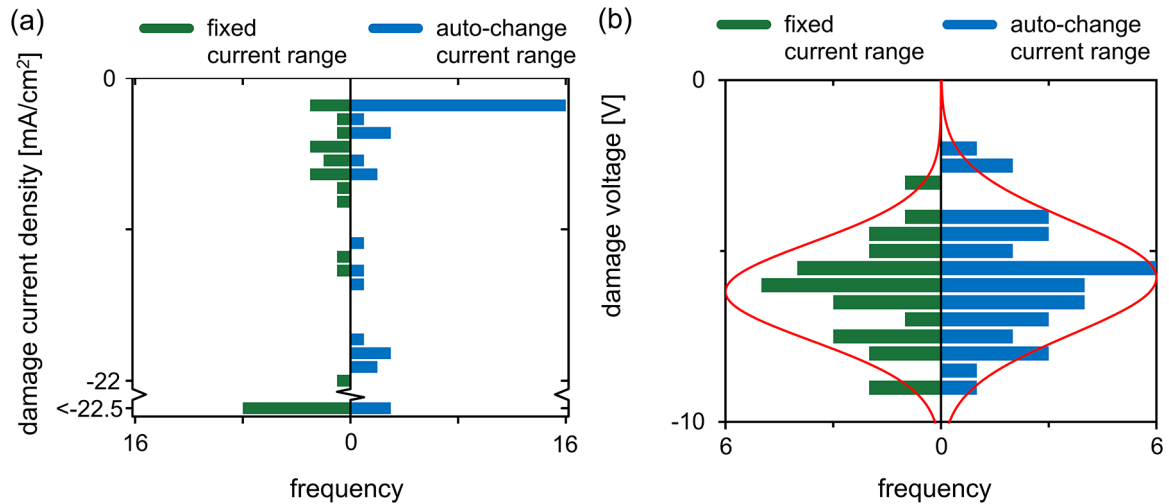


**Fig. A.1.** (a) Histograms of damage current density in dark reverse bias sweeps with on the left results of fixed current range and on the right the auto-change current range results. The last bin (bottom) represents the number of cells with a damage current density smaller than  $-22.5 \text{ mA/cm}^2$ . (b) Histograms of damage voltage in dark reverse bias sweep and the normal distribution curve based on average and standard deviation for measurements performed with fixed and auto-change current range.